The International Archives of the Photogrammetry, Remote Sensing and Spatial Information Sciences, Volume XLVIII-1/W6-2025
3rd International Workshop on Evaluation and BENCHmarking of Sensors, Systems and
GEOspatial Data in Photogrammetry and Remote Sensing (GEOBENCH), 20–21 November 2025, Wroclaw, Poland

Assessing the photogrammetric potential of a smartphone device with integrated dual-frequency GNSS

Mohamedelmustafa Omer Eid[1,2], Luca Morelli[1], Fabio Remondino[1]

[1] 3D Optical Metrology (3DOM) unit, Bruno Kessler Foundation (FBK), Trento, Italy
Web: http://3dom.fbk.eu – Email: (meid, lmorelli, remondino)@fbk.eu
[2] Department of Civil, Building and Environmental Engineering (DICEA), Sapienza University of Rome, Italy

Keywords: Low-Cost, Smartphone, dual-frequency, RTK, GNSS-Assisted Photogrammetry, Xiaomi 13T

Abstract
Photogrammetric 3D surveys generally rely on high-end professional cameras and ground control points, whose placement and measurement can be time-consuming, error-prone, or even hazardous in inaccessible environments. GNSS-assisted photogrammetry provides a viable alternative by directly linking image capture with centimetre-level GNSS positioning, eliminating the need for GCPs. However, such systems typically rely on high-end cameras and professional GNSS equipment, which are costly, bulky, and demand expert operation. Recent advances in smartphone technology, combining high-resolution cameras, multi-frequency GNSS, and inertial sensors, suggest the potential for these devices to function as integrated platforms for low-cost, lightweight, and accessible photogrammetric surveying. Despite challenges related to antenna quality, signal noise, and limited documentation of sensor characteristics, post-processing strategies have shown that smartphones can achieve decimetre- to centimetre-level positioning accuracy under favourable conditions. This study investigates the performance of an Android smartphone equipped with a dual-frequency (L1, L5) GNSS receiver and high-resolution camera as a standalone device for terrestrial photogrammetry. The research evaluates its capacity to deliver metrically accurate, georeferenced 3D models without external surveying instruments, thereby assessing the feasibility of smartphones as a compact, cost-effective alternative to professional-grade systems in field mapping applications.

1. Introduction

Photogrammetry reconstructs 3D data from overlapping images, defined up to an arbitrary scale and reference system. These data may then be scaled for metric purposes as well as geo-referenced e.g. using ground control points (GCPs), but their placement in the field can be laborious or unfeasible due to environmental constraints. In addition, field work and collimation in photogrammetric software are time-consuming and prone to operator errors. GNSS-assisted photogrammetry avoids GCPs' usage through coupling a GNSS receiver and a camera to directly assign metric 3D coordinates to camera centers and therefore georeference and scale the photogrammetric model. This method is especially useful in aerial mapping applications (Skaloud et al., 1996; Zhou et al., 2018; Tomaštík et al., 2019). It requires a calibration of the lever arm of the antenna phase center (APC) and the centre of projection (COP) of the camera (Forlani et al., 2014; Morelli et al., 2022).
Typically, professional reflex cameras and surveying level equipment (i.e., high-end GNSS receivers and/or total stations) are used to acquire the data, but these systems can be expensive, the equipment can be bulky and therefore slow down operations in the field and often require trained professionals for proper use. To minimize survey cost and time, integrated devices with low-cost GNSS receivers and cameras have been suggested as a lightweight alternative to geodetic grade equipment (Nocerino et al., 2012; Morelli et al., 2022; Oniga et al., 2024; Previtali et al., 2024; Wieser et al., 2024; Běloch et al., 2025). But these solutions still rely on specialized equipment whereas smartphones offer a more compact and accessible alternative, in particular for 3D reconstruction purposes (Nocerino et al., 2017; Torresani and Remondino, 2019; Barbero-Garcia et al., 2021). Moreover, continuous improvements in smartphone cameras, together with integrated sensors (e.g., IMU and GNSS) have made them a compact device that could - in theory - replicate the functionality of specialized equipment, thereby reducing both cost and survey effort for various applications (Corradetti et al., 2021).

Previous works have directly employed GNSS positions estimated internally by the smartphone in single point positioning (SPP), in combination with IMU-derived orientation measurements, to register image networks and achieving errors of 2-10 meters (Tavani et al., 2020; Tavani et al., 2022), or in conjunction with total station controls reducing the errors to decimeters (Shan et al., 2023). Analyses of raw GNSS data from smartphones indicate that, compared to geodetic-grade receivers under similar conditions, they exhibit lower signal-to-noise ratios (SNR), higher pseudo-range noise, irregular satellite tracking and frequent cycle slips. These limitations necessitate careful data acquisition - such as proper phone mounting, extended observation periods, use of ground planes to reduce multipath effects, and disabling other interfering sensors - as well as meticulous data processing (Paziewski et al., 2021; Zangenehnejad and Gao, 2021; Everett et al., 2022; Tomaštík and Everett, 2023). For post-processed kinematic (PPK) positioning, these issues must be carefully considered, along with additional uncertainties stemming from the limited documentation of smartphone GNSS capabilities, as detailed specifications (tracked constellations, frequencies, carrier-phase observables, or antenna phase center offsets) are not published by manufacturers. The device's GNSS receiver capabilities (tracked constellations and number of frequencies) can be retrieved using the GPSTest[1] application, while some researchers have attempted to calibrate the antenna phase center (Netthonglang et al., 2019; Wanninger et al., 2020; Shen et al., 2024), although this offset is not consistent across devices, therefore, each device needs independent calibration.
Nevertheless, post-processing strategies can be tuned to account for the higher noise characteristics and antenna limitations of smartphones, as well as unflagged multipath effects that are typically handled more robustly by geodetic and even low-cost receivers (Everett et al., 2022). As demonstrated in some works (Paziewski et al., 2021; Odolinski et al., 2024; Pourmina et al., 2024), when such adaptations are applied, both static and kinematic positioning can achieve decimeter- to centimeter-level accuracy.

[1] https://github.com/barbeau/gpstest

1.1 Aim of the study

This study evaluates the capability of the Android -based Xiaomi 13T smartphone, equipped with high-resolution cameras and a dual-frequency (L1, L5) GNSS receiver, as a sole device for terrestrial photogrammetry. In particular, we aim to investigate whether the device could be feasible to replace professional cameras and conventional surveying equipment for georeferencing and scaling purposes.
To the best of the author's knowledge, this is the first study to evaluate this approach using solely the smartphone camera and its integrated GNSS receiver, while simultaneously targeting centimetre-level accuracy with PPK processing. Previous studies have either focused exclusively on assessing GNSS accuracy in RTK/PPK modes, or on integrating cameras with GNSS operating in SPP mode.

2. Methodology

The data collected by the smartphone consists of an image block acquired following photogrammetric practice and raw GNSS data, which are then processed in PPK mode. The estimated 3D coordinates are directly assigned to the centre of projection (COP) of the acquired images to scale and georeference the photogrammetric block. The APC and the COP are assumed coincident. This assumption is supported by previous research on devices from the same manufacturer (Xiaomi), which estimated the antenna's position near the upper part of the smartphone (Wanninger et al., 2020; Shen et al., 2024), within a rectangular area of approximately 3x7cm with a depth of <1cm, in which the camera is centred. Therefore, the error associated with this assumption is on the order of 2-3 cm, which is smaller than the accuracy attainable with RTK/PPK using a smartphone under the setup and acquisition times employed in the experiments reported in this paper.
The same smartphone image block georeferenced with an F9R ublox - a centimeter-level low-cost GNSS receiver - is used as a reference for comparison. In this case, indirect georeferencing is adopted using GCPs. The evaluation is conducted at two sites in Trento (Italy), to assess the repeatability and robustness of the proposed approach.

Figure 1. Samples of the acquired images at Site 1.

2.1 Test sites

The first site features a façade of a small building (Figure 1), a scenario with favourable satellite visibility and minimal signal obstruction. A set of 33 images are acquired at ca 4.5m distance from the façade, with an average 2.6 mm GSD. 18 points (Figure 4) - 12 natural points and 6 screws installed in the asphalt - are used as control and check points (9 and 9, respectively).
The second site (Figure 2) features a higher and more complex building. Although the area generally offers open-sky conditions, partial signal blockage from the southern direction occurs due to the height of the surveyed building. This site therefore serves as a more challenging scenario, with moderate GNSS signal degradation. In this site, a set of 223 images are acquired at ca 10-14 m distance from the façade, with an average 4.2 mm GSD. 6 points well distributed on the ground (Figure 5) are used as control points and check points (3 and 3 respectively).

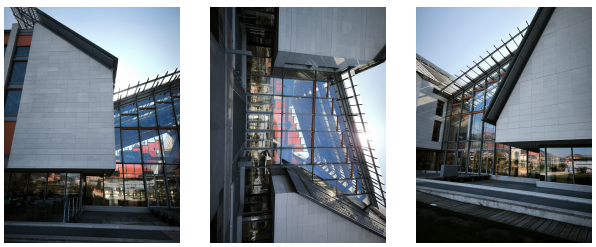

Figure 2. Samples of the acquired images at Site 2.

2.2 Reference data acquisition and processing

In both sites, an image set is acquired using the Xiaomi 13T, orthogonal and oblique with respect to the main façade, including landscape and portrait image orientations.

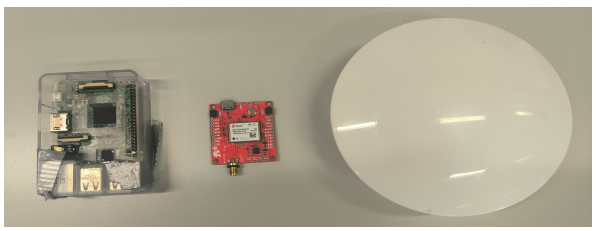

Figure 3. GNSS reference data acquisition system: the Raspberry Pi 2 (left), the ublox ZED-F9R module and the TOP 106 antenna (right).

Moreover, ground truth GNSS data are collected with a TOPGNSS antenna TOP106 mounted on a geodetic pole with a known fixed height, with the antenna connected to a ublox ZED-F9R low-cost receiver. Raw data are collected and stored with a Raspberry Pi 2 (Figure 3). The acquired points are processed in PPK using dual-frequency (L1/L2) observations from a base station (MOCA) located ca 4-5 km from the surveyed buildings. The base station's receiver tracks L1/L2 observations from GPS, Galileo and GLONASS, although GLONASS observations are discarded as they are shown to degrade the solution. The survey lasted 3-5 minutes at each point and the data are processed using RTKLIB demo5 (Everett et al., 2022), a version of RTKLIB (Takasu, 2009) optimized for low-cost GNSS receivers. The pole height and the APC offset are both compensated in the position estimation. The GNSS points are divided into control and check points, and the photogrammetric block is oriented in Agisoft Metashape using the positions of the control points to constrain the bundle block adjustment (BBA), while the interior orientation parameters are estimated in self-calibration.

2.3 Smartphone raw GNSS data collection and processing

Using the Xiaomi 13T internal GNSS antenna, a set of 3D points is surveyed at each test site. Each point is surveyed for ca 10 min and at each point an image is acquired. These images are added to the reference image block acquired (Section 2.2) and their COPs constrained on estimated PPK positions from the phone's

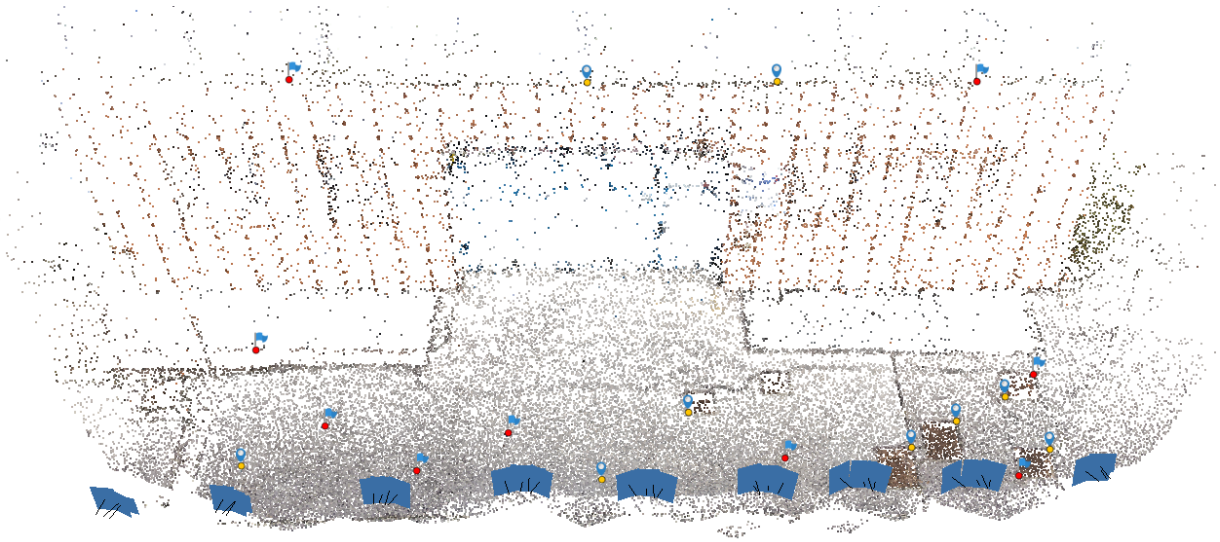

Figure 4. Overview of Site 1 façade reference reconstruction with camera network (blue frames), GCPs (red points) and check points (yellow points).

GNSS. This process allows to directly georeference and scale the image block in a process called GNSS-assisted photogrammetry without the use of GCPs. In addition, the smartphone-based coordinates can be directly compared with the GCPs coordinates to evaluate smartphone GNSS accuracy decoupled from the photogrammetric processing (see Section 3).

The smartphone acquires dual-frequency raw observations (L1 and L5) from GPS and Galileo as well as single-frequency observations (L1) from BeiDou and GLONASS. Since the MOCA base station uses a receiver that does not track GPS L5 and BeiDou observations, the PPK solution is estimated using observations from a base station (ROVE) located ca 21 km away from the surveyed buildings that also collects L5 data. While differential positioning over longer baselines (>20 km) can result in slightly reduced accuracy - typically up to decimeters (Magalhães et al., 2021) - the richer set of observations available at ROVE base station compensates for the potential loss of accuracy due to the extended baseline. A comparison of the positioning errors obtained using each base station is provided in Section 3.2.

Two GNSS data acquisition modalities are tested: the first with the smartphone mounted on a tripod and the second by putting the smartphone on the ground with its camera facing the façade. The first modality represents the conventional surveying method for photogrammetric applications, while the latter limits signal reflections arriving from multiple directions (e.g. the ground).

The data are processed in RTKLIB demo5 using static mode with a forward filter and predicted orbits to approximate real-time data processing. Elevation masks are set at 32° for L1 and 25° for L5 to reduce low-elevation noise while retaining enough observations. Cycle slip detection using the doppler measurements (comparing the expected carrier phase change from Doppler with the measured change) is applied with a threshold of 5. For the rest of the parameters, the default settings[2] are utilized. For the elevated points (using a tripod or a pole), using the abovementioned settings resulted in spurious fixes, indicating noisier raw data. Looking at the raw observations, we observed that - as opposed to geodetic receivers - signal strength is not proportional to satellite elevation and lower satellites can have a higher signal-to-noise (SNR) ratio, as also reported by the analysis in Paziewski et al. (2021). Thus, while the elevation masking threshold of SNR is usually consistent across a single frequency (e.g., 32 for L1 and 25 for L5), in this case, SNR data are analyzed prior to setting the SNR masking threshold and thus, a separate threshold is defined for each elevation bin (10-degrees interval). This process is applied to each observation file. Although it is a time-consuming process, it helps filtering out weaker observations while preserving enough measurements for solution estimation, which is particularly important given the lower number of satellites tracked and the higher noise present in smartphone data.

To account for instable "fix" status, a "fix" (i.e., the solution where the carrier-phase integer ambiguities have been successfully resolved) is considered "valid" only if the position remains in "fix" status for at least 10 consecutive seconds. Once this 10-second fixed period is reached, all subsequent position fixes are averaged to produce the final position estimate.

2.4 Smartphone-based 3D reconstruction with PPK

Only a subset of the entire image block has PPK positions, this subset is used to constrain the BBA of the image network from Section 2.1, without using any additional GCPs, while a set of check points are used to verify the reconstruction accuracy.

The RMSE on the checkpoints is compared with the RMSE obtained from the reference reconstruction georeferenced with GCPs acquired with the ublox F9R + TOP106 antenna.

In the first test site 6 photos and their raw GNSS observations are acquired (Figure 6), whereas in Site 2, 13 photos and their raw GNSS observations are acquired (Figure 7).

2.5 Evaluation metrics

The evaluation is done on two different levels: first, the smartphone GCP coordinates are computed by projecting the measured positions from a known height down to the ground plane, allowing a direct comparison with the ground truth coordinates (Section 3). Secondly, the images with their GNSS coordinates are used to scale and georeference the photogrammetric models obtained using the same image network as in Section 2.1. The statistics on the check points are estimated and reported in comparison to the ublox model (Section 4).

[2] https://rtklibexplorer.wordpress.com/2021/02/27/another-look-at-l1-l5-cellphone-ppk-with-rtklib/

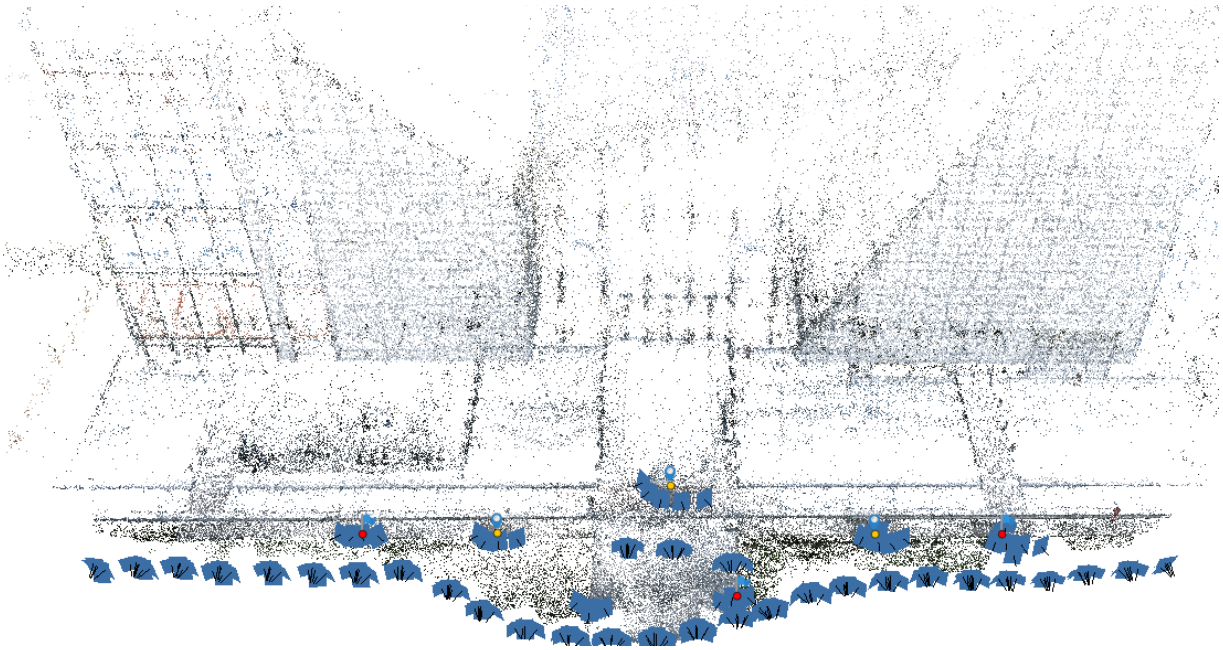

Figure 5. Overview of Site 2 façade reference reconstruction with camera network (blue frames), GCPs (red points) and check points (yellow points).

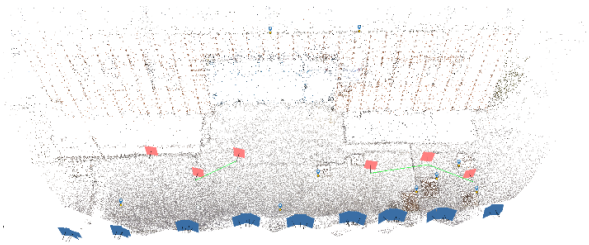

Figure 6. Dense point cloud of the façade in Site 1 obtained using the 6 smartphone georeferenced images (in red).

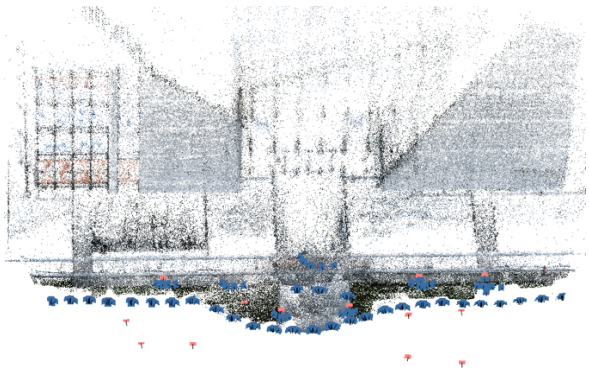

Figure 7. Dense point cloud of Site 2 obtained using the 13 smartphone georeferenced images (in red).

3. Accuracy evaluation

The accuracy of the GNSS integrated within the smartphone, independently from the photogrammetric process, is assessed by comparing the estimated position with that of a centimetre-level GNSS (ublox F9R receiver coupled with a TOP106 antenna) operating in RTK mode, which serves as the ground truth.
In Section 3.1, tests are conducted using a short baseline of approximately 1 km from the nearest permanent station (ROVE) and a longer baseline (ca 21 km) to test different configurations for data acquisitions. On the other hand, Section 3.2 reports the accuracy evaluation at the two sites employed for the photogrammetric processing.

3.1 GNSS accuracy evaluation under different smartphone configurations

Two acquisition modalities are tested: one with the smartphone mounted on a tripod/pole (elevated configuration) and another with the device placed on the ground with its longitudinal axis orthogonal to the ground (ground-fixed configuration). Three test points are selected, for which the ground truth coordinates re surveyed using the ublox F9R. All three points are situated in areas with clear sky visibility with Point 3 located at a short distance from the GNSS base station (ca 1 km) and Points 1 and 2 located at a considerably greater distance (ca 21 km). At each point, two consecutive 10 minutes acquisitions are performed, one for each acquisition modality (elevated and ground-fixed configurations), guaranteeing comparable satellite geometry and signal conditions. Table 1 reports the time to first fix (TTFF), the percentage of fixed solutions and the error in East, North, and Up (E, N, U) directions for each acquisition modality.

Point (modality)	TTFF [s]	E [cm]	N [cm]	U [cm]
1 (tripod)	434	1.8	-2.2	9.3
1 (ground)	74	-0.4	-1.9	8.0
2 (tripod)	No fix	-	-	-
2 (ground)	197	-3.6	-4.1	13.2
3 (tripod)	No fix	-	-	-
3 (ground)	88	1.0	0.6	4.7

Table 1. Comparison between two acquisition modalities in three different points.

The results reported in Table 1 show that the elevated (tripod-mounted) configuration degrades positioning accuracy, with respect to the ground-fixed configuration that reach in all cases centimetre level accuracy for the three components. The underlying cause remains uncertain. It may result from an interaction with the tripod or, more likely, from the elevated position of the phone, which enables signals from below to reach the phone's antenna.

This shows the smartphone receiver's limited capability to suppress multipath effects when exposed to reflected signals from the surrounding environment, while the ground setup inherently limits the reception of these faulty reflected signals.

3.2 GNSS accuracy evaluation

Firstly, we had to determine the most suitable permanent GNSS station by considering both its distance and the availability of frequencies and constellations. Sections 3.2.1 and 3.2.2 present the tests conducted in the two different sites to assess positional accuracy using the selected permanent base station.
The smartphone raw GNSS data from Site 1 are processed in PPK (described in Section 2.3) using observations from two different base stations. Table 2 summarizes the positioning results of the 9 control points using a base station at 4 km (MOCA) and at 21 km (ROVE), reporting the tracked frequencies (1/2/5) per constellation - GPS (G), Galileo (E), GLONASS (R) and BeiDou (C), the average TTFF, number of valid points (i.e., points with 10 consecutive fixes) and the mean 2D error on the valid points.

Station	G	E	R	C	TTFF [s]	Valid points	2D err [cm]
MOCA 4-5 km	1/2	1/2/5	1/2	-	333	5/9	43.0
ROVE 21 km	1/2 /5	1/2/5	1/2	1/2	310	7/9	13.0

Table 2. PPK solution comparison between MOCA and ROVE solutions 3D positioning errors.

As reported in Table 2, the solution from MOCA demonstrates longer TTFF, less valid points and lower 2D accuracy, mainly due to the lower number of tracked frequencies (no GPS L5) and constellations (no BeiDou). Thus, PPK solutions obtained using ROVE are utilized in the following. Although dual-frequency observations typically result in a faster time to first fix (TTFF) than reported in Table 2, in our study we consider as valid "fix" a solution that remains in "fix" for at least 10 consecutive epochs, thus, delaying the time to first fix.

3.2.1 Site 1 façade

Nine check points are surveyed under identical conditions with the smartphone mounted on a tripod. Two points failed to achieve a valid fix, indicating a certain variability under apparent "stable" conditions, maybe suggesting interference from other smartphone sensors or in any case demonstrating great sensitivity to slight changes in signal reception conditions.
To estimate horizontal and vertical errors of the fixed solutions, smartphone control point coordinates are transformed into local Cartesian (E, N, U). Only the points with valid "fixes" are shown in Figure 8. The E, N and U error statistics of the measured points are reported in Table 3.

Errors	Mean [cm]	Max [cm]	RMSE [cm] All points	RMSE [cm] Without outliers
E	11.9	43.7	17.6	6.7
N	2.4	4.6	2.8	2.8
U	12.2	60.6	23.5	5.6

Table 3. Errors of Xiaomi coordinates of control points in Site 1.

As reported in Section 3.1, the use of a tripod rarely resulted in a fixed solution due to increased observational noise. Therefore, to obtain a fix in scenarios where the tripod was used for a better sky visibility, a detailed post-processed kinematic (PPK) analysis of the observations and residuals is required to identify and exclude the satellites that prevented the fix. The RMSE, calculated treating only a point as an outlier, exhibited component-wise variations in error between the 2.8 and 6.7 cm.

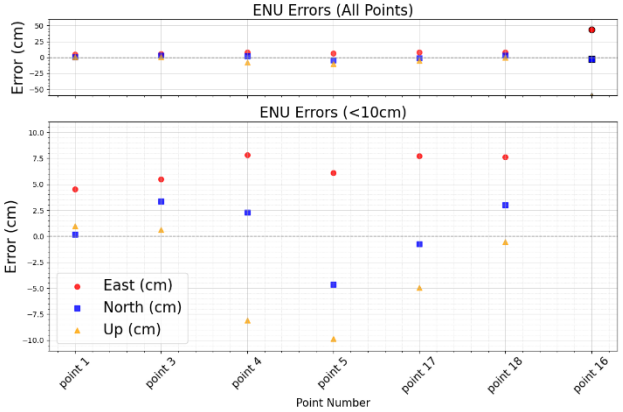

Figure 8. East (in red), North (in blue) and Up (in yellow) errors of the seven control points.

3.2.2 Site 2 façade

The same evaluation is carried out on five control points of Site 2 and compared with the ublox solution. Two points reported an error of >10cm in one the of the positioning components (E, N, U) and are classified as outliers (Figure 9). The E, N and U error statistics of the inlier measured points are reported in Table 4.

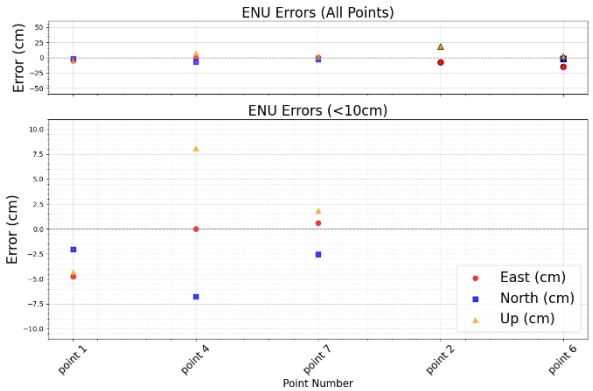

Figure 9. East (in red), North (in blue) and Up (in yellow) errors of the seven control points.

Errors	Mean [cm]	Max [cm]	RMSE [cm] All points	RMSE [cm] Without outliers
E	5.6	14.9	7.8	2.8
N	30.7	140	63.0	4.3
U	7.0	19.0	9.5	5.4

Table 4. Errors of Xiaomi coordinates of control points in Site 2.

Although three out of five points exhibited significantly higher errors than the others at this stage, the fixed solutions are obtained differently from Site 1, i.e. without additional processing or cleaning of the observations. Consequently, this approach yielded consistent GNSS positions with the smartphone, achieving sub-decimetre accuracy.

4. Smartphone PPK to scale and georeference photogrammetric data

Whereas the previous section assessed the accuracy of GNSS positioning independently, without integrating image data, this section evaluates the potential of directly georeferencing a photogrammetric block using smartphone data. At this scope, a limited

number of smartphone images with their GNSS coordinates are added to a wider image block without GNSS coordinates, since every GNSS acquisition require 5/10 min of data logging. The GNSS coordinates added as constraints in the BBA allow a scaled and georeferenced 3D reconstruction. A-priori accuracy of COPs has been set to 8 and 15 cm for horizontal and vertical components, respectively. The accuracy of the reconstruction is assessed evaluating the RMSE on a set of check points. The `smartphone approach` is compared against the classical methodology of indirect georeferencing using a set of ground control points and checked on the same check points used for the `smartphone approach`. Both ground control points and checkpoints have been acquired with the ublox F9R and the TOP106 antenna.

4.1 Site 1 façade

Six images acquired at 2-3m distance from the façade with an average GSD of <2mm are used to georeference the photogrammetric model (Figure 6). Table 5 reports the RMSE of the check points for the ublox model (reference) and the Xiaomi model.

Model	No. of points	XY RMSE [cm]	Z RMSE [cm]	Total RMSE [cm]
ublox	9	1.0	1.8	2.1
Xiaomi		10.0	8.1	12.9

Table 5. RMSEs on the check points from ublox and Xiaomi models in Site 1.

The Xiaomi model has a higher total RMSE, both in the XY plane, with a difference of 9 cm, and in the Z direction, with a difference of ca 6 cm.

4.2 Site 2 façade

13 images are acquired at ca 7-15m from the façade with an average GSD of 3.8 mm are used to georeference the photogrammetric model (Figure 7), the statistics on the check points are reported in Table 6. In line to the previous paragraph, the Xiaomi model has a higher total RMSE, both in the XY plane and in the Z direction.

Model	No. of points	XY RMSE [cm]	Z RMSE [cm]	Total RMSE [cm]
ublox	3	1.6	1.1	1.9
Xiaomi		7.3	3.3	8.0

Table 6. RMSEs on the check points from ublox and Xiaomi models in Site 2.

Furthermore, in both sites, features on the surveyed façades are measured with a mm-level calliper to serve as check for the 3D model scale (Table 7), with mean errors under centimetre level.

Site	Ground truth scale bar distance [cm]	Mean error [cm]	Maximum deviation [cm]
#1	99 (3 objects)	0.7	0.9
#2	100 (2 objects)	0.3	0.4
	125 (1 object)		

Table 7. Scale validation in the two sites.

5. Conclusions

This study evaluated the potential of a dual-frequency off-the-shelf smartphone as a standalone device for GNSS-assisted photogrammetry, aiming to replace conventional surveying instruments coupled with cameras.

Employing the smartphone's internal antenna, the resulting 3D data achieved a total RMSE at a decimetre level on check points. This accuracy corresponds to a restitution scale of approximately 1:300 for 2D technical drawings. When interpreting this result, it should be noted that the decimetre-level error reflects the use of the smartphone's GNSS both for scaling and georeferencing the image block. A significant improvement in model accuracy can be achieved by introducing scale bars, which allow scaling at the millimetre level, while georeferencing would remain at the decimetre level (in case of a baseline of ca 20 km from the nearest reference station).

The obtained results are encouraging, considered the long distance to the GNSS permanent base station and the uncertain position of the internal antenna phase center (APC), suggesting room for improvement to move from decimetre to centimeter level accuracy. Indeed, while the RMSE reaches the decimetre level in photogrammetric experiments over long baselines (Section 4), the short-baseline experiment (Section 3.1) yields results close to the ground truth positions provided by the u-blox F9R (point 3 on the ground). Only one experiment is reported in the paper, but this finding are confirmed by repeating the experiment three additional times on the same point across different days.

With respect to signal quality and robustness, acquisition campaigns conducted on points in close proximity and over short time intervals can exhibit considerable variability in both fix acquisition and positional accuracy, probably related to a high sensitivity of the smartphone integrated GNSS receiver to external environmental conditions. Placing the smartphone directly on the ground reduces this variability and substantially limits the need for data cleaning during post-processing, such as the inspection of observations and residuals. For this issue, future work will focus on using materials or shielding structures capable of attenuating reflected signals that allow the smartphone to be positioned on a tripod while maintaining favourable signal reception conditions.

The smartphone demonstrated longer TTFF, thus required longer acquisition times than professional equipment, but its ubiquity, high-resolution cameras and centimeter-level GNSS capability still make it a viable alternative for many photogrammetric applications. Inconsistencies in fixed solutions under apparently identical conditions must be further investigated, e.g. improving data acquisition to suppress multipath or performing dedicated antenna phase centre calibration with shorter baselines to isolate and mitigate smartphone-specific limitations. The TTFF analysis also suggests that, under favourable sky conditions and with the smartphone placed on the ground, a static acquisition time of five minutes may be sufficient, instead of the ten minutes adopted in the experiments.

While this study focuses on static processing, the evaluation of kinematic accuracy will be an important direction for future research, potentially following an initial static initialization phase. Such an approach could simplify data acquisition and enable new application scenarios.

References

Barbero-García, I., Pierdicca, R., Paolanti, M., Felicetti, A., Lerma, J.L., 2021. Combining machine learning and close-range photogrammetry for infant's head 3D measurement: A smartphone-based solution. *Measurement*, 182.

Běloch, L. and Pavelka, K., 2025. Low-Cost solution for kinematic mapping using spherical camera and GNSS. *Applied Sciences*, *15*(11), p. 5972.

Corradetti, A., Seers, T. D., Billi, A., & Tavani, S. 2021. Virtual outcrops in a pocket: The smartphone as a fully equipped photogrammetric data acquisition tool. *GSA TODAY*, 31(9), 4-9.

Everett, T., Taylor, T., Lee, D. K., Akos, D. M. 2022. Optimizing the use of RTKLIB for smartphone-based GNSS measurements. *Sensors*, 22(10), 3825.

Forlani, G., Pinto, L., Roncella, R. and Pagliari, D., 2014. Terrestrial photogrammetry without ground control points. *Earth Science Informatics*, 7(2), pp.71-81.

Magalhães, A., Bastos, L., Maia, D. and Gonçalves, J.A., 2021. Relative positioning in remote areas using a GNSS dual frequency smartphone. *Sensors*, 21(24), p.8354.

Morelli, L., Menna, F., Vitti, A., Remondino, F., 2022. Action cams and low-cost multi-frequency antennas for GNSS assisted photogrammetric applications without ground control points. *Int. Arch. Photogramm. Remote Sens. Spatial Inf. Sci*., XLVIII2/W1-2022, 171-176.

Netthonglang, C., Thongtan, T., Satirapod, C., 2019. GNSS Precise positioning determinations using smartphones. Proc. *IEEE Asia Pacific conference on circuits and systems (APCCAS),* pp. 401-404.

Nocerino, E., Menna, F., Remondino, F., 2012. GNSS/INS aided precise re-photographing. Proc. 18th *IEEE VSMM*, pp. 235-242.

Nocerino, E., Poiesi, F., Locher, A., Tefera, Y. T., Remondino, F., Chippendale, P., and Van Gool, L., 2017. 3D reconstruction with a collaborative approach based on smartphones and a cloud-based server. *Int. Arch. Photogramm. Remote Sens. Spatial Inf. Sci.*, XLII-2/W8, 187-194.

Odolinski, R., Yang, H., Hsu, L. T., Khider, M., Fu, G. M., & Dusha, D. 2024. Evaluation of the multi-GNSS, dual-frequency RTK positioning performance for recent android smartphone models in a phone-to-phone setup. Proc. *International Technical Meeting of The Institute of Navigation*, pp. 42-53.

Oniga, E., Boroianu, B., Morelli, L., Remondino, F. and Macovei, M., 2024. Beyond ground control points: cost-effective 3D building reconstruction through GNSS-integrated photogrammetry. *Int. Arch. Photogramm. Remote Sens. Spatial Inf. Sci*., *48*, pp. 333-339.

Paziewski, J., Fortunato, M., Mazzoni, A., & Odolinski, R. 2021. An analysis of multi-GNSS observations tracked by recent Android smartphones and smartphone-only relative positioning results. *Measurement*, 175, 109162.

Pourmina, A. H., Alizadeh, M. M., & Schuh, H. 2024. Decimeter-level accuracy for smartphone real-time kinematic positioning implementing a robust kalman filter approach and inertial navigation system infusion in complex urban environments. *Sensors*, 24(18), 5907.

Previtali, M., Barazzetti, L., and Roncoroni, F., 2024. GNSS assisted photogrammetric reconstruction from combined 360° videos and UAV images. *Int. Arch. Photogramm. Remote Sens. Spatial Inf. Sci*., XLVIII-2/W4-2024, 365-372.

Shan, J., Li, Z., Lercel, D., Tissue, K., Hupy, J., & Carpenter, J. 2023. Democratizing photogrammetry: an accuracy perspective. *Geo-Spatial Information Science*, 26(2), 175-188.

Shen, F., Hu, Q., & Gong, C. (2024). Determining the antenna phase center for the high-precision positioning of smartphones. *Sensors*, 24(7), 2243.

Skaloud, J., Cramer, M., Schwarz, K., 1996. Exterior orientation by direct measurement of camera position and attitude. *Int. Arch. Photogramm. Remote Sensing*, *31*, 125-130.

Takasu, T., 2009. RTKLIB: Open source program package for RTK-GPS. *Proceedings of the FOSS4G*, *1*, pp.1-6.

Tavani, S., Billi, A., Corradetti, A., Mercuri, M., Bosman, A., Cuffaro, M., Seers, T., Carminati, E. 2022. Smartphone assisted fieldwork: Towards the digital transition of geoscience fieldwork using LiDAR-equipped iPhones. *Earth-Science Review*s, 227, 103969.

Tavani, S., Pignalosa, A., Corradetti, A., Mercuri, M., Smeraglia, L., Riccardi, U., Seers, T., Pavlis, T., Billi, A. 2020. Photogrammetric 3d model via smartphone GNSS sensor: Workflow, error estimate, and best practices. *Remote Sensin*g, 12(21), 3616.

Tomaštík, J., & Everett, T. 2023. Static positioning under tree canopy using low-cost GNSS receivers and adapted RTKLIB software. *Sensors*, 23(6), 3136.

Tomaštík, J., Mokroš, M., Surový, P., Grznárová, A., & Merganič, J. (2019). UAV RTK/PPK Method - An optimal solution for mapping inaccessible forested areas? *Remote Sensing*, *11*(6), 721.

Torresani, A. and Remondino, F., 2019. Videogrammetry vs photogrammetry for heritage 3D reconstruction. *Int. Arch. Photogramm. Remote Sens. Spatial Inf. Sci.,* XLII-2/W15, 1157-1162.

Wanninger, L. and Heßelbarth, A., 2020. GNSS code and carrier phase observations of a Huawei P30 smartphone: Quality assessment and centimeter-accurate positioning. *GPS Solutions*, *24*(2), 64.

Wieser, M., Verhoeven, G., Wild, B. and Pfeifer, N., 2024. Exterior Orientation in a Box: Cost-Effective RTK/IMU-Based Photo Geotagging. *Int. Arch. Photogramm. Remote Sens. Spatial Inf. Sci*., *48*, pp. 463-470.

Zangenehnejad, F., & Gao, Y. 2021. GNSS smartphones positioning: Advances, challenges, opportunities, and future perspectives. *Satellite navigation*, 2(1), 24.

Zhou, Y., Rupnik, E., Faure, P.-H., Pierrot-Deseilligny, M., 2018. GNSS-Assisted Integrated Sensor Orientation with Sensor Pre-Calibration for Accurate Corridor Mapping. *Sensors*, *18*, 2783.